Sustainable Energy & Fuels

Coupling FeNi Alloys and Hollow Nitrogen-Enriched Carbon Framework Leads to High-Performance Oxygen Electrocatalysis for Rechargeable Zinc-Air Battery

Journal:	*Sustainable Energy & Fuels*
Manuscript ID	SE-ART-07-2018-000362.R2
Article Type:	Paper
Date Submitted by the Author:	30-Aug-2018

Complete List of Authors:	Wu, Haihong; Chinese Academy of Sciences, Lanzhou Institute of Chemical Physics Zeng, Min; Chinese Academy of Sciences, Lanzhou Institute of Chemical Physics Li, Zhiyun; Chinese Academy of Sciences, Lanzhou Institute of Chemical Physics Zhu, Xiang; Texas A&M University College Station, Chemistry Tian, Chengcheng; University of Tennessee, Xia, Chungu; Lanzhou Institute of Chemical Physics, Chinese Academy of Sciences, He, Lin; Chinese Academy of Sciences, Lanzhou Institute of Chemical Physics Dai, Sheng; Oak Ridge National Laboratory,

Journal Name

ARTICLE

Coupling FeNi Alloys and Hollow Nitrogen-Enriched Carbon Framework Leads to High-Performance Oxygen Electrocatalysis for Rechargeable Zinc-Air Battery

Received 00th January 20xx,
Accepted 00th January 20xx

DOI: 10.1039/x0xx00000x

www.rsc.org/

Haihong Wu,[†a,b] Min Zeng,[†a] Zhiyun Li,[†a] Xiang Zhu,[*,c] Chengcheng Tian,[d] Chungu Xia,[*,a] Lin He[*,a] and Sheng Dai[d]

A dual-template strategy for facile preparation of a bifunctional oxygen electrocatalyst for high-performance rechargeable Zinc-air batteries was reported. Coupling FeNi alloys with hollow nitronge-doped carbon frameworks results in exceptionally high electrocatalytic oxygen reduction and evolution activities. In 1 M KOH, the resulting new material exhibits a superior oxygen evolution activity with a low overpotential of 250 mV to deliver 10 mA cm^{-2} current density, where the obtained oxygen reduction performance is also comparable to that of the commercial Pt/C and the half-wave potential reaches as high as 0.87 V. As a result, bifunctional oxygen electrocatalysis performance thus obtained (0.61 V, 1 M KOH) ranks among the best of non-precious oxygen electrocatalysts. Using this new catalyst as an air electrode, the as-prepared rechargeable Zn-air battery shows a high current of 215 mA cm^{-2} at a voltage of 1.0 V, large peak power density (310 mW cm^{-2}), high potential efficiency (64.7 % at 10 mA cm^{-2}) and prolonged operation durability. This approach provides a means to control the surface features, thereby tuning the catalytic property of the material and may open up new possibilities for the rational design and synthesis of new materials for electrochemical applications.

Introduction

The development of renewable energy generation and storage systems, such as rechargeable metal-air batteries, is vital for mitigating the adverse effects of the increasing global energy crisis and environmental issues.[1-3] Zn-air batteries have attracted tremendous attention due to their high theoretical energy density of 1086 Wh kg^{-1}, low cost and environmentally friendly components, suggesting great promise for application in portable electronic devices and electric vehicles.[4-10] However, their energy efficiencies are still far from satisfying and have been significantly limited by large overpotentials derived from the sluggish oxygen reduction reaction (ORR) and oxygen evolution reaction (OER) kinetics at the air cathode.[11, 12] Thus far, precious Pt-based materials and Ru/Ir-based compounds are state-of-the-art electrocatalysts for the ORR and OER, respectively; however, their intrisnic drawbacks, such as high cost and poor durability, have restricted their potential scale-up preparation.[1-3] In this regard, great research efforts have been devoted to the rational design and synthesis of highly efficient and cost-effective bifunctional oxygen electrocatalysts for Zn-air batteries.

Among various types of catalysts, transition-metals (e.g. Fe, Co, Ni) and their derivatives (such as FeCo and FeNi alloys) have been studied as promising alternatives because of their theoretically high catalytic activities and rich reserves.[13, 14] However, solely using these materials usually results in poor bifunctional oxygen catalytic performance. For example, FeNi and FeCo alloys have been extensively studied for the OER, whereas their ORR activities were shown to be very low owing to the lack of ORR-active sites within the architectures.[15-20] In this context, coupling these nanoparticles with ORR-active nitrogen-doped carbon (N-C) materials, to work in concert, could be a promising methodology to improve their bifunctional electrocatalytic performance.[21-24] Unfortunately, merging these two different kinds of attractive sites in one material remains a challenge, mainly because it is difficult to bridge over their huge synthesis differences.

Herein, we report a dual-template strategy to create FeNi alloys and hollow N-C framework hybrid as an efficient bifunctional electrocatalyst for the OER and ORR in alkaline media. The key of our success lies in the formation of an attractive FeNi-based core-shell nanostructure by the thermal treatment of a FeNi-based Prussian blue analogue. The core-shell structures further give rises to forming hollow N-C frameworks by simply acidic etching of FeNi nanoparticles. As a result, the obtained new catalyst exhibits an excellent OER activity in 1 M KOH with a low overpotential (η_{10}) of

[a] *State Key Laboratory for Oxo Synthesis and Selective Oxidation, Suzhou Research Institute of Lanzhou Institute of Chemical Physics, Chinese Academy of Sciences, Lanzhou, 730000, China, Email:* cgxia@licp.cas.cn; helin@licp.cas.cn;
[b] *University of Chinese Academy of Sciences, Beijing 100049, China*
[c] *Department of Chemistry, Texas A&M University, College Station, Texas, 77843, USA,* Email: xiang@tamu.edu/zhuxiang.ecust@gmail.com;
[d] *Chemical Sciences Division, Oak Ridge National Laboratory, Oak Ridge, TN 37831, USA*
† These authors contributed equally to this work
Electronic Supplementary Information (ESI) available: [details of any supplementary information available should be included here]. See DOI: 10.1039/x0xx00000x

250 mV to deliver 10 mA cm^{-2} current density, where the ORR activity is also comparable to the commercial Pt/C and the half-wave potential ($E_{1/2}$) reaches as high as 0.87 V. Additionally, using the catalyst as an air electrode, the obtained rechargeable Zn-air battery exhibits a high current of 215 mA cm^{-2} at a voltage of 1.0 V, large peak power density (310 mW cm^{-2}) and prolonged operation stability

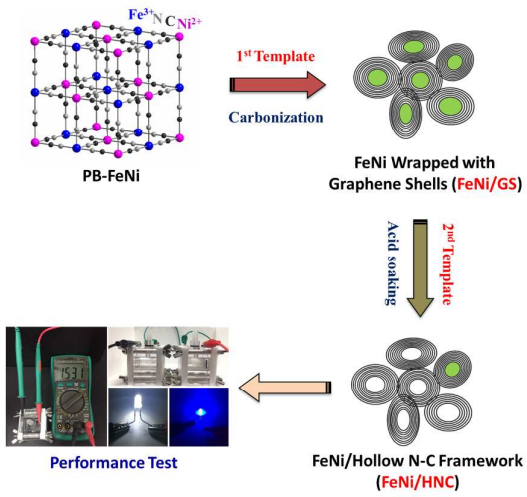

Scheme 1. Schematic illustration of the synthesis of **FeNi/HNC** from the FeNi-containing Prussian blue (PB-FeNi) and digital photo for the application of home-made rechargeable Zn-air battery.

Results and discussion

As shown in **Scheme 1**, FeNi-based Prussian blue analogue (PB-FeNi), was prepared and employed as the sacrificial template. A simple coprecipitation of nickel acetate and $K_3Fe(CN)_6$ solutions affords the formation of PB-FeNi nanoparticles (Synthesis details can be found in the supporting information).[25] The structural features of PB-FeNi were first studied by the X-ray diffraction (XRD) technique. As shown in **Fig. 1a**, the pattern for PB-FeNi matches well with that of Nitrosyl Nickel Iron Cyanide Hydrate $Ni[Fe(CN)_5NO]_2{\cdot}2H_2O$ (JCPDS card no. 00-022-0463). A high carbon yield of *ca.* 40 wt% (over 600 °C) was indicated by the thermogravimetric analysis (TGA) (Fig. S1). Pyrolysis at 600 °C under Ar was subsequently performed to convert PB-FeNi to the desired FeNi alloys wrapped with graphene-like shells (**FeNi/GS**).

The formation of graphitic structure was supported by the observed D (*ca.* 1346 cm^{-1}) and G band (*ca.* 1580 cm^{-1}) in Raman spectroscopy of **FeNi/GS** (**Fig. 1e**).[26] Graphene-like shell with an interlayer distance of 3.40 Å, was clearly observed by the high-resolution transmission electron microscopy (HR-TEM) image (**Fig. 1d**). Most importantly, the existence of FeNi alloys was indicated by the XRD pattern (JCPDS card no. 00-012-0736) (**Fig. 1a**). This result was further confirmed by the HR-TEM measurement. As shown in **Fig. 1d**, an obvious lattice fringe with a d-spacing of 2.06 Å, consistent with the (111) plane of the FeNi alloy, was observed. Energy dispersive X-ray spectroscopy (EDS) confirms the presence of Fe, Ni, C and N within the material (**FeNi/GS**). Interestingly, mapping of their relative distributions indicates the presence of the N-doped graphene-like shells as well (Fig. S2).

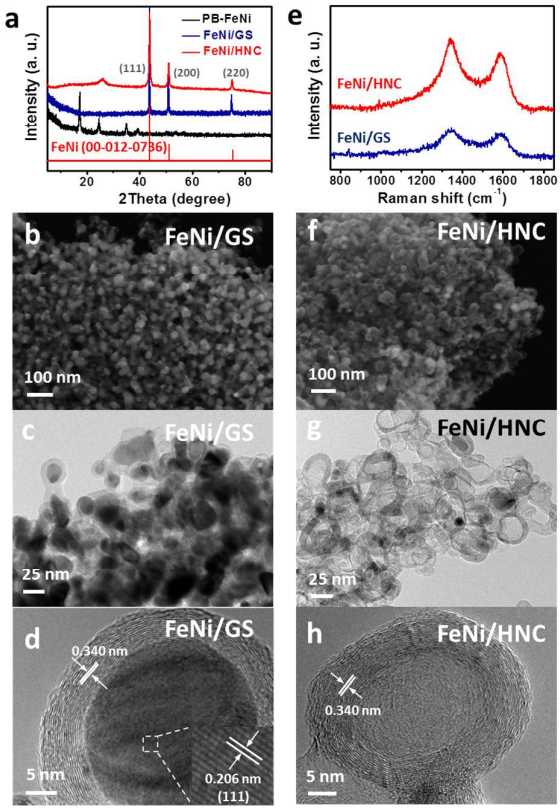

Fig. 1. (a) XRD patterns of PB-FeNi, **FeNi/GS** and **FeNi/HNC**. (b-d) SEM and TEM images of FeNi/GS; the inset in (e) is the enlarged high resolution TEM image showing the lattice fringe of FeNi (111). (e) Raman spectra of **FeNi/GS** and **FeNi/HNC**. (f-h) SEM and TEM images of **FeNi/HNC**.

We then examined the OER activity on the **FeNi/GS** in 1 M KOH using a typical rotating disc electrode (RDE) technique. A glassy carbon was employed as the working electrode (catalyst loading: *ca.* 0.3 mg cm^{-2}). As expected, a high catalytic activity for the OER was achieved as a result of the existence of rich FeNi alloys, exceeding that of the commercial noble Ir/C catalyst. **Fig. 2a** displays linear sweep voltammetry (LSV) curves. The anodic current recorded on the **FeNi/GS** renders a sharp onset potential at 1.34 V (versus reversible hydrogen electrode, RHE), which is better than that of the Ir/C (E_{onset} = 1.44 V). The overpotential (η_{10}) on **FeNi/GS** to deliver 10 mA cm^{-2} current density, which is a metric related to solar water-splitting devices, reaches as low as 266 mV. This value is lower than that of Ir/C (η_{10}= 275 mV) and also comparable to the best-performing non-precious OER catalysts, for example NiCo

bimetal-organic framework nanosheets (η_{10}= 250 mV),[27] Ni_2P/NiO_x core-shell structure (η_{10}= 280 mV)[28] and Co_4N porous nanowire arrays (η_{10}= 257 mV)[29]. A detailed comparison of various highly active OER catalysts is shown in Table S1.

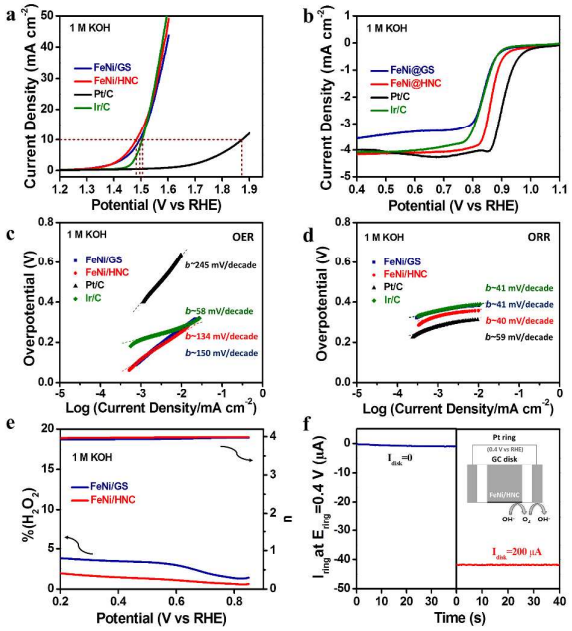

Fig. 2. RDE disk polarization curves of the OER and ORR for **FeNi/GS**, **FeNi/HNC**, Pt/C and Ir/C in both 1 M KOH (a and b). The corresponding Tafel plots of OER (c) and ORR (d) for **FeNi/GS**, **FeNi/HNC**, Pt/C and Ir/C, respectively. (e) Calculated peroxide yield and electron transfer number of **FeNi/GS** and **FeNi/HNC** in O_2 saturated 1 M KOH from the RRDE disk polarization curves. (f) The ring current of **FeNi/HNC** on RRDE in N_2 saturated 1 M KOH solution (ring potential: 0.4 V).

Motivated by the above promising OER performance**,** we further studied the ORR performance in 1.0 M KOH. The polarization of **FeNi/GS** curve on the rotating ring disk electrode (RRDE) exhibits a positive onset potential (E_{onset}) of 0.98 V and a high half-wave potential ($E_{1/2}$) of 0.84 V (**Fig. 2b**), which is 70 mV smaller than that of the 20 wt% commercial Pt/C (E_{onset}= 1.06 V and $E_{1/2}$= 0.91 V). We reasoned that the lack of active ORR sites within the matrix may account for this lower performance. As reported, N-doped graphene materials have been extensively studied as alternative efficient metal-free ORR catalysts.[6, 30] We thus hypothesized that selective etching of FeNi alloys inside **FeNi/GS** by acid solutions towards the formation of hollow N-doped carbon frameworks could help to improve the overall ORR performance.

Toward this end, the as-obtained **FeNi/GS** was further used as a second template. After simply etching with 1 M HCl for 8 h, significant mass losses of both Fe (10.2 vs 22.7 wt%) and Ni (15.1 vs 34.5 wt%) were obtained for the new material (**FeNi/HNC**) based on the inductively coupled plasma (ICP) analysis. Acidic etching with longer time of 16 h affords the lowest content of Fe and Ni (Table S6). In turn, the porosity of the resultant material was greatly enhanced (177 $m^2\ g^{-1}$ for **FeNi/HNC** and 38 $m^2\ g^{-1}$ for **FeNi/GS**), as confirmed by the N_2 adsorption-desorption curves at 77 K (Fig. S3). The obtained pore size distribution curves successfully support the existence of mesopores within the matrix of **FeNi/HNC**. Highly porous architecture could help to facilitate the gas and electrolyte to the active sites, thereby boosting the ORR performance. Furthermore, HR-TEM images clearly indicates the generation of hollow carbon framework (**Fig. 1g** and **h**), where some OER-active FeNi alloys wrapped with graphene-like layers were also observed. The XRD result supports the existence of FeNi alloys as well (**Fig. 1a**). X-ray photoelectron spectroscopy (XPS) was thus performed to study the surface chemical features. As depicted in Fig. S4a and S4b, the lowest binding energy peaks in both Ni and Fe spectra correspond to metallic Ni (852.7 eV) and Fe (707.2 eV) from FeNi alloys. The peak at 853.8 eV and 855.4 eV is ascribed to Ni ($2P_{3/2}$) of Ni^{2+} and Ni^{3+}, respectively. And, the Fe 2P spectrum shows two peaks at 709.7 eV and 712.7 eV.[31-33] In addition, high N containing of 4.1 at% was obtained for the **FeNi/HNC**. And two major N species, including pyridinic and pyrrolic N, were existed. Accordingly, high ORR activity on this new mesoporous **FeNi/HNC** with hollow N-enriched carbon frameworks could be expected.[34-36]

The RRDE test was performed in 1.0 M KOH by using the **FeNi/HNC** as a new electrode material so as to evaluate its ORR activity. Interestingly, the **FeNi/HNC** exhibits an enhanced ORR activity with a $E_{1/2}$ of 0.87 V, which is only 40 mV lower than that of the Pt/C. Moreover, the Tafel slope of **FeNi/HNC** (40 mV dec^{-1}) is lower than that of Pt/C (59 mV dec^{-1}) (**Fig. 2d**), suggesting a faster kinetic process. The excellent ORR activity of **FeNi/HNC** is comparable to previously-reported high-performance non-precious catalysts (Table S2). The CV curves under N_2 and O_2 atmospheres as well as RDE polarization curves in 1 M KOH at different electrode rotation speeds are recorded and shown in Fig. S6, further confirming the obtained high activity. We reasoned that the existence of rich N-doped hollow spheres and intrinsic mesoporous nature of **FeNi/HNC** may account for this enhanced performance. The peroxide yield was measured to be lower than 5.0 % at all potentials (**Fig. 2e**). As a result, a high electron transfer number (> 3.9) is calculated, suggesting a four-electron reduction of oxygen.

Although some FeNi alloys were removed by acidic washing, the OER performance on the **FeNi/HNC** maintains very well. The new material affords a current density of 10 mA cm^{-2} at 1.48 V with an exceptional overpotential (η_{10}) of 250 mV. We further examined the effect of etching time on the OER activity, where no significant progress was achieved when the etching time was extended to 16 h (Fig. S7). Nevertheless, the fact that the existence of FeNi alloys plays a crucial role in achieving such a high OER activity can be confirmed by poison testing (Fig. S8). In the presence of KSCN, significant loss of OER activity with a much higher overpotential (340 mV) was obtained for the **FeNi/HNC** due to the coordination between FeNi sites and SCN^- anions. Additionally, the use of 1 M KOH/5 mM KSCN as the electrolyte affords a decreased ORR activity as well.

Tafel plots were then examined to study the intrinsic catalytic kinetics of the OER on the **FeNi/HNC**. The Tafel slope value of **FeNi/HNC** (134 mV dec^{-1}) is lower than that of **FeNi/GS** (150 mV dec^{-1}), but still higher than that of Ir/C (58 mV dec^{-1}) (**Fig. 2c**). A

more detailed investigation of the reaction mechanism, using the rotating ring-disk electrode (RRDE) technique with a Pt ring electrode potential of 1.50 V (RHE), was carefully performed.[37] Under this condition, the peroxide intermediates generated at the **FeNi/HNC** surface during the OER can be oxidized. Negligible hydrogen peroxide formation was indicated by a very low ring current (<6 μA) (Fig. S9). Thus, a four electron pathway for water oxidation: i.e., $4OH^- \rightarrow O_2+2H_2O+4e^-$ can be suggested.[37] Additionally, we further employed a RRDE with a ring potential of 0.40 V (RHE) to reduce the generated O_2, rendering a continuous OER (disk electrode) → ORR (ring electrode) process, to further verify the resulting current originates from the OER rather than other side reactions.[37-39] As shown in **Fig. 2f**, when the disk current at 0 (i_{disk}=0) was applied, negligible ring current was obtained. However, the constant use of disk current at 200 μA (I_{disk}=200 μA) successfully afforded a ring current of ~ 41.6 μA, indicating that the generated O_2 molecules were quickly reduced.[37] Therefore, the oxidation current originates from the OER with a high Faradaic efficiency of 98 %. The obtained promising OER performance may be further supported by the electrochemical active surface area (ECSA) of **FeNi/HNC**, which was evaluated by the electrochemical double-layer capacitance (C_{dl}) and surface roughness factor (R_f).[40-43] As shown in Fig. S10, the C_{dl} and R_f of **FeNi/HNC** was determined to be 12.8 mF cm^{-2} with an R_f value of 213.3, which are three times higher than that of **FeNi/GS** (C_{dl}= 3.9 mF cm^{-2} and Rf = 65.0). The ECSA is therefore calculated to be 71.1 m^2 g^{-1}, when a specific capacitance value *C*s = 0.060 mF cm^{-2} is adopted.[44] High ECSA value of **FeNi/HNC** further confirm its favorable reaction kinetics since previous works have demonstrated that large ECSA could facilitate the access of electrolyte into the catalytically active surfaces.[45]

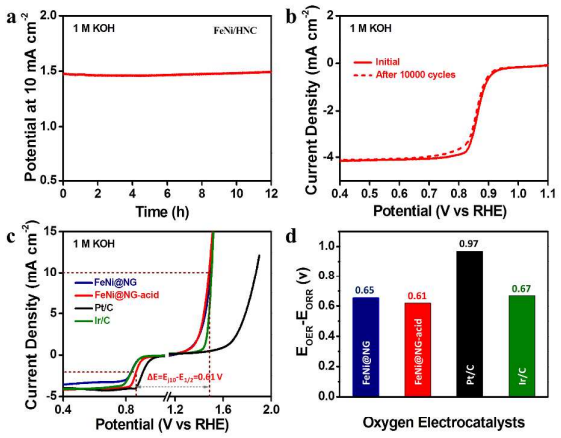

Fig. 3. (a) Potential-time curve at a constant current density of 10 mA cm^{-2} for **FeNi/HNC** in 1 M KOH. (b) Polarization curves for the ORR activity of **FeNi/HNC** before and after 10000 cylces. (c) RDE disk polarization curves of OER and ORR for **FeNi/GS**, **FeNi/HNC**, Pt/C and Ir/C in 1 M KOH. (d) The difference in potential between OER current density at 10 mA cm^{-2} and the half-wave potential of ORR for **FeNi/GS**, **FeNi/HNC**, Pt/C and Ir/C.

Durability has been considered as another key parameter governing long-term practical application of electrocatalysts in energy conversion and storage systems. The potential of **FeNi/HNC** shifted positively less than 20 mV to maintain 10 mA cm^{-2} for 12 hours and negligible ORR performance loss was observed after 10000 cycles, suggesting prolonged operation stabilities (**Fig. 3a** and **3b**). The overall oxygen electrocatalytic activity on **FeNi/HNC** was evaluated by the difference of OER and ORR metrics ($\Delta E=E_{j=10} - E_{1/2}$). The smaller ΔE value is, the closer the catalyst is to an ideal reversible oxygen electrode.[5] As shown in **Fig. 3c-d** and Table S3, the ΔE obtained for the **FeNi/HNC** (0.61 V) is among the best, suggesting high potential application as electrode materials for rechargeable Zn-air battery.

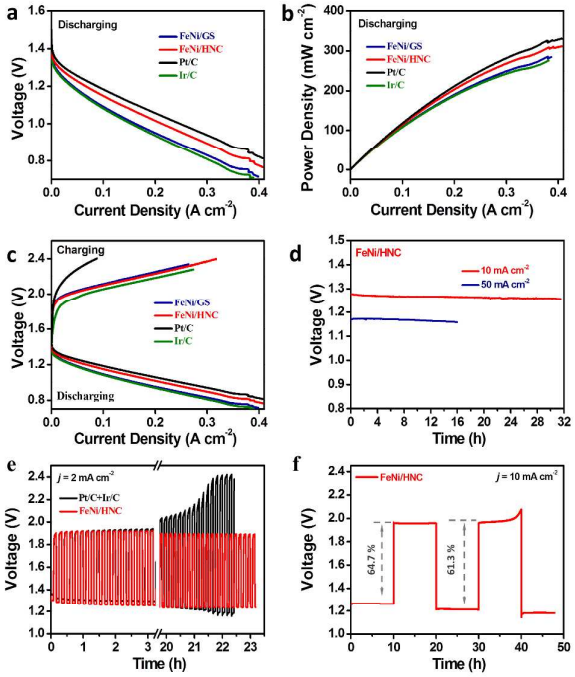

Fig. 4. The electrochemical performance of zinc-air batteries. Discharge polarization curve (a) and corresponding power density (b) of zinc-air batteries using **FeNi/GS**, **FeNi/HNC**, Pt/C and Ir/C as the air catalyst. (c) Discharge and charge polarization curves of rechargeable zinc-air batteries with different electrocatalysts. (d) Long-time galvanostatic discharge curves of zinc-air batteries using **FeNi/HNC** as the air catalyst at 10 mA cm^{-2} and 50 mA cm^{-2}. (e) Cycling performance of rechargeable zinc-air battery with **FeNi/HNC** and Pt/C/Ir/C at 2 mA cm^{-2}. (f) Cycling data at 10 mA cm^{-2} in long cycle periods (20 hours per cycle). The catalyst loading is 1 mg cm^{-2} on carbon paper.

FeNi/HNC was then studied as the air cathode material to evaluate the battery performance (Fig. S12, detailed information can be found in the supporting information). 6 M KOH solution was employed as the electrolyte, and an open circuit voltage of *ca.* 1.43 V (**Fig. 4a**) was obtained for the home-made zinc-air battery. The

polarization curve and corresponding power density plot was shown in **Fig. 4 a** and **b**. Remarkably, a large current density of 215 mA cm^{-2} is delivered at a voltage of 1.0 V. The maximum power density reaches as high as 310 mW cm^{-2}, ranking among the best performance (Table S4). Furthermore, an exceptionally high stability was also observed for our zinc-air battery. When galvanostatically discharged at a current density of 10 mA cm^{-2} for 32 h, even 50 mA cm^{-2} for 16 h, no obvious voltage drop was observed (**Fig. 4d**). The slight voltage loss is associated with the degradation of zinc anode. As shown **Fig. 4e**, the **FeNi/HNC** shows a long cycle life of over 23 hours without any obvious voltage change. In contrast, the controlled Zn-air battery prepared by using Pt/C and Ir/C as electrode materials exhibits very poor cycle life with a large overpotential increase. When galvanostatic charge and discharge curves were performed at higher current density of 10 mA cm^{-2} and a longer cycle period of 20 hours, promising cycle performance with a small overpotential increase of 70 mV was obtained for the **FeNi/HNC** as well (**Fig. 4f,** Table S5). A high voltage efficiency of 64.7 % and 61.3 % was achieved, respectively.

Conclusions

In summary, a dual-template strategy was developed to generate a high-performance bifunctional oxygen electrocatalyst for rechargeable Zinc-air batteries. The key of our success lies in the simultaneous installation of OER-active FeNi alloys and ORR-active N-doped hollow carbon within one material framework. The resulting new catalyst exhibits an excellent oxygen evolution activity with a low overpotential of 250 mV to deliver 10 mA cm^{-2} current density in 1 M KOH, where the obtained ORR performance is comparable to the commercial Pt/C and the half-wave potential reaches as high as 0.87 V. As a result, the bifunctional performance thus obtained for the new material (0.61 V, 1 M KOH) ranks among the best of non-precious oxygen electrocatalysts. Furthermore, using the catalyst as the desired air electrode material, the as-prepared rechargeable Zn-air battery exhibits a high current of 215 mA cm^{-2} at a voltage of 1.0 V, large peak power density (310 mW cm^{-2}), high potential efficiency (64.7 % at 10 mA cm^{-2}) and prolonged operation durability. This approach provides a means to control the surface features, thereby tuning the catalytic property of the material and may open up new possibilities for the rational design and synthesis of new materials for electrochemical applications.

Acknowledgements

This research was supported financially by National Program for Thousand Young Talents of China, National Natural Science Foundation of China (21633013, 21703267) and Foundation research project of Jiangsu Province (BK20171242, BK20170423).

Notes and references

1. Z. L. Wang, D. Xu, J. J. Xu and X. B. Zhang, *Chem. Soc. Rev.*, 2014, **43**, 7746-7786.
2. F. Cheng and J. Chen, *Chem. Soc. Rev.*, 2012, **41**, 2172-2192.
3. Y. Li and H. Dai, *Chem. Soc. Rev.*, 2014, **43**, 5257-5275.
4. Y. Li, M. Gong, Y. Liang, J. Feng, J. E. Kim, H. Wang, G. Hong, B. Zhang and H. Dai, *Nat. Commun.*, 2013, **4**, 1805.
5. T. Y. Ma, J. Ran, S. Dai, M. Jaroniec and S. Z. Qiao, *Angew. Chem. Int. Ed.*, 2015, **54**, 4646-4650.
6. J. Zhang, Z. Zhao, Z. Xia and L. Dai, *Nat. Nanotechnol.*, 2015, **10**, 444-452.
7. Q. Liu, Y. Wang, L. Dai and J. Yao, *Adv. Mater.*, 2016, **28**, 3000-3006.
8. X. Liu, M. Park, M. G. Kim, S. Gupta, G. Wu and J. Cho, *Angew. Chem. Int. Ed.*, 2015, **54**, 9654-9658.
9. L. Li and A. Manthiram, *Adv. Energy Mater.*, 2016, **6**, 1502054.
10. J. Fu, D. U. Lee, F. M. Hassan, L. Yang, Z. Bai, M. G. Park and Z. Chen, *Adv. Mater.*, 2015, **27**, 5617-5622.
11. Y. Zheng, Y. Jiao, Y. Zhu, Q. Cai, A. Vasileff, L. H. Li, Y. Han, Y. Chen and S.-Z. Qiao, *J. Am. Chem. Soc.*, 2017, **139**, 3336-3339.
12. T. Cheng, W. Bin, W. Hao-Fan and Z. Qiang, *Adv. Mater.*, 2017, **29**, 1703185.
13. W. T. Hong, M. Risch, K. A. Stoerzinger, A. Grimaud, J. Suntivich and Y. Shao-Horn, *Energy Environ. Sci.*, 2015, **8**, 1404-1427.
14. F. Song, L. Bai, A. Moysiadou, S. Lee, C. Hu, L. Liardet and X. Hu, *J. Am. Chem. Soc.*, 2018, **140**, 7748-7759.
15. U. Y. Qazi, C. Z. Yuan, N. Ullah, Y. F. Jiang, M. Imran, A. Zeb, S. J. Zhao, R. Javaid and A. W. Xu, *ACS Appl. Mater. Interfaces*, 2017, **9**, 28627-28634.
16. G. Zhang, G. Wang, H. Liu, J. Qu and J. Li, *Nano Energy*, 2018, **43**, 359-367.
17. Y. Yang, Z. Lin, S. Gao, J. Su, Z. Lun, G. Xia, J. Chen, R. Zhang and Q. Chen, *ACS Catal.*, 2017, **7**, 469-479.
18. X. Zhu, T. Jin, C. Tian, C. Lu, X. Liu, M. Zeng, X. Zhuang, S. Yang, L. He, H. Liu and S. Dai, *Adv. Mater.*, 2017, **29**, 1704091.
19. P. Cai, Y. Hong, S. Ci and Z. Wen, *Nanoscale*, 2016, **8**, 20048-20055.
20. F. Gengtao, C. Zhiming, C. Yifan, L. Yutao, T. Yawen and G. J. B., *Adv. Energy Mater.*, 2017, **7**, 1601172.
21. G. L. Tian, M. Q. Zhao, D. Yu, X. Y. Kong, J. Q. Huang, Q. Zhang and F. Wei, *Small*, 2014, **10**, 2251-2259.
22. J. Wang, H. Wu, D. Gao, S. Miao, G. Wang and X. Bao, *Nano Energy*, 2015, **13**, 387-396.
23. C. Hu and L. Dai, *Angew. Chem. Int. Ed.*, 2016, **55**, 11736-11758.
24. G. Wu, A. Santandreu, W. Kellogg, S. Gupta, O. Ogoke, H. Zhang, H. L. Wang and L. Dai, *Nano Energy*, 2016, **29**, 83-110.
25. M. Zeng, Y. Liu, F. Zhao, K. Nie, N. Han, X. Wang, W. Huang, X. Song, J. Zhong and Y. Li, *Adv. Funct. Mater.*, 2016, **26**, 4397-4404.
26. Z. Zhang, M. Dou, H. Liu, L. Dai and F. Wang, *Small*, 2016, **12**, 4193-4199.
27. S. Zhao, Y. Wang, J. Dong, C. T. He, H. Yin, P. An, K. Zhao, X. Zhang, C. Gao, L. Zhang, J. Lv, J. Wang, J. Zhang, A. M. Khattak, N. A. Khan, Z. Wei, J. Zhang, S. Liu, H. Zhao and Z. Tang, *Nat. Energy*, 2016, **1**, 16184.
28. L. A. Stern, L. Feng, F. Song and X. Hu, *Energ. Environ. Sci.*, 2015, **8**, 2347-2351.
29. P. Chen, K. Xu, Z. Fang, Y. Tong, J. Wu, X. Lu, X. Peng, H. Ding, C. Wu and Y. Xie, *Angew. Chem. Int. Ed.*, 2015, **54**, 14710-14714.
30. D. Guo, R. Shibuya, C. Akiba, S. Saji, T. Kondo and J. Nakamura, *Science*, 2016, **351**, 361-365.
31. G. Wu, W. Chen, X. Zheng, D. He, Y. Luo, X. Wang, J. Yang, Y. Wu, W. Yan, Z. Zhuang, X. Hong and Y. Li, *Nano Energy*, 2017, **38**, 167-174.
32. V. Gomez, S. Irusta, O. B. Lawal, W. Adams, R. H. Hauge, C. W. Dunnill and A. R. Barron, *RSC Adv.*, 2016, **6**, 11895-11902.
33. Z. Zhao, H. Wu, H. He, X. Xu and Y. Jin, *J. Mater. Chem. A*, 2015, **3**, 7179-7186.
34. X. Zhu, Y. Zhu, C. Tian, T. Jin, X. Yang, X. Jin, C. Li, H. Wang, H. Liu and S. Dai, *J. Mater. Chem. A*, 2017, **5**, 4507-4512.
35. Y. Li, T. Li, M. Yao and S. Liu, *J. Mater. Chem.*, 2012, **22**, 10911-10917.

36. J. C. Li, P. X. Hou, S. Y. Zhao, C. Liu, D. M. Tang, M. Cheng, F. Zhang and H. M. Cheng, *Energy Environ. Sci.*, 2016, **9**, 3079-3084.
37. T. Y. Ma, S. Dai, M. Jaroniec and S. Z. Qiao, *J. Am. Chem. Soc.*, 2014, **136**, 13925-13931.
38. T. Y. Ma, J. L. Cao, M. Jaroniec and S. Z. Qiao, *Angew. Chem. Int. Ed.*, 2016, **55**, 1138-1142.
39. D. Chen, C. L. Dong, Y. Zou, D. Su, Y. C. Huang, L. Tao, S. Dou, S. Shen and S. Wang, *Nanoscale*, 2017, **9**, 11969-11975.
40. D. U. Lee, J. Y. Choi, K. Feng, H. W. Park and Z. Chen, *Adv. Energy Mater.*, 2014, **4**, 1301389.
41. Y. Li, P. Hasin and Y. Wu, *Adv. Mater.*, 2010, **22**, 1926-1929.
42. K. Gong, F. Du, Z. Xia, M. Durstock and L. Dai, *Science*, 2009, **323**, 760-764.
43. J. Tian, Q. Liu, A. M. Asiri and X. Sun, *J. Am. Chem. Soc.*, 2014, **136**, 7587-7590.
44. C. C. L. McCrory, S. Jung, J. C. Peters and T. F. Jaramillo, *J. Am. Chem. Soc.*, 2013, **135**, 16977-16987.
45. H. Kong, J. Song and J. Jang, *Chem. Commun.*, 2010, **46**, 6735-6737.

TOC

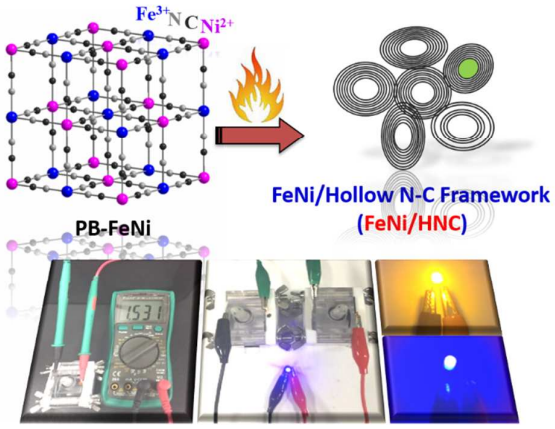

A dual-template strategy for facile preparation of a bifunctional oxygen electrocatalyst for high-performance rechargeable Zinc-air batteries was reported.